BUTTERWORTH HEINEMANN

Polymer Vol. 36 No. 4, pp. 821–836, 1995

0032-3861/95/$10.00+0.00

A temperature window of reduced flow resistance in polyethylene with implications for melt flow rheology: 2. Rheological investigations in the extrusion window

J. W. H. Kolnaar* and A. Keller†
H. H. Wills Physics Laboratory, University of Bristol, Bristol BS8 1TL, UK
(Received 24 November 1993; revised 18 July 1994)

The present part of this series on the temperature window of reduced flow resistance in polyethylene confirms and consolidates the inference from the first paper in this series that the source of the rheological singularity resides in the capillary, specifically at the capillary wall, in contrast to the previously held view that the elongational flow at the entrance is responsible for the effect. The experimental material leading to this conclusion comprises the varying of the angle of the entrance orifice and of the capillary dimensions (length and diameter), the use of a constrictionless parallel barrel and also of an orifice without a capillary in the various extrusion experiments, together with the use of different materials of construction for the capillary. The results of each of these examinations are detailed in this paper. In addition to leading to the above conclusion, these studies extended the rheological examination of polyethylene melts, specificaly to the unusual rheological behaviour associated with the temperature window of reduced flow resistance which has been explored as a function of the above variables. Amongst others, the effects in the capillary have been separated from those in the entry orifice, providing an unexpected new approach to the exploration of flow instabilities to be pursued in the next paper of this series. The source of the temperature window is discussed in the light of the above findings with reaffirmation of its origin as a phase transformation induced by chain extension along the capillary wall. Attention is drawn to the wider implications beyond the confines of the rather special circumstances of the present experiments.

(Keywords: capillary extrusion; melt flow sinuglarity; reduced flow resistance)

INTRODUCTION

This is the second part of a series of three papers. In the first part[1], we reported on a narrow temperature interval at around 150°C, occurring during capillary extrusion of high molecular weight polyethylene, in which extrusion pressures are anomalously low and in which an extrudate is obtained possessing a smooth surface finish and comparatively little die swell. This 'temperature window' at 150°C is present at rates of extrusion at which under conventional conditions, i.e. at higher temperatures, several kinds of extrudate distortion are observed.

In line with preceding works from this laboratory[2–5], the origin of this melt flow singularity around 150°C was attributed to a thermodynamic factor – more specifically, to a phase transition at the particular temperature. The formation of a transient, hexagonal, 'mobile' crystal phase was suggested, as created through flow-induced chain extension.

In the first part of this series, the effects of the extrusion parameters – temperature, pressure and rate – and polymer molecular weight on the temperature window were investigated[1]. Here the extrusion temperature (T) was varied, i.e. it was continuously increased or decreased, with the pressure (p) being recorded. In *Figure 1* pressure (p) vs. temperature (T) traces are given as a function of piston velocity (v), showing the basic effect in question: at and beyond a critical rate v_c a sharp minimum in pressure is found to set in, becoming more pronounced, but with its location remaining essentially unaltered, with increasing rate of extrusion (*Figure 1* has been reproduced from the first paper in this series for self-contained presentation).

It was further shown in the first paper in this series that the critical rate for the onset of the minimum, such as in *Figure 1*, is strongly dependent on molecular weight (M). Using samples with different weight average molecular weights ($M_w \equiv M$) and comparable molecular weight distributions, it was found that the critical piston displacement rate at the onset of the pressure minimum (v_c) obeyed a negative fourth power relationship in M (i.e. $v_c \propto M^{-4.0}$).

In contrast, the pressure drop at the onset of the pressure minimum in *Figure 1* (p_c) was found to be independent of M. Also, when extrusion was maintained at a fixed pressure level (i.e. stress) and the temperature

* Permanent address: DSM Research BV, Koestraat, PO Box 18, 6160 MD Geleen, The Netherlands
† To whom correspondence should be addressed

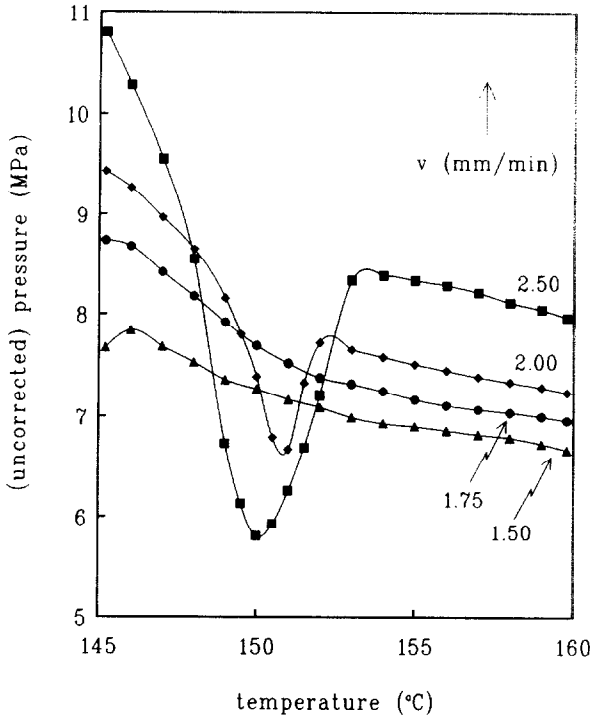

Figure 1 Pressure (uncorrected) vs. temperature traces for several values of increasing piston velocity (v), showing the onset of the pressure minimum (capillary $L/D = 14/2$, $2\alpha = 90°$)

of extrusion was slowly lowered, a sharp maximum in extrusion rate was found to set in beyond p_c at the temperature of around 150°C, where p_c was, in a first approximation, independent of M. This new finding indicated to us that the initiation of the window effect is likely to be in the capillary; more specifically, the invariance of p_c may point to a yield phenomenon, such as slippage along the capillary wall.

The prime objective of the present paper is to lend weight to the above assertion, namely that the source of the basic effect is not in the entry zone but within the capillary. This would mean that it is not associated with elongational flow, which arises through convergence at the orifice – a view held in preceding publications, in line with all previous evidence on elongational flow induced crystallization effects as first observed by van der Vegt and Smit[6] – but flow within the capillary. Since in the capillary flow is parallel to the stationary walls, it must possess a strong transverse velocity gradient, which accordingly would have to be responsible for the window effect. It would thus follow that near the walls, flow can have a special influence on the chain, which in turn produces a change from parabolic-type flow to (partial) plug flow, which, as we already inferred in the first part of this series, would be the source of the effects in question.

For the above purpose we take the following three experimental routes: (1) we vary the entrance geometry, specifically the entrance angle (α) for given capillary dimensions; (2) we vary the capillary length (L) and diameter (D) for a fixed entrance geometry; and (3) we study the role of the material from which the capillary is constructed.

All the above will bear out the correctness of our earlier[1] inference, namely that the source of the special effects in question is indeed within the capillary portion of the flow field. In addition, with the criticalities in the parameters as identified earlier[1] being satisfied, we assert that the effects are associated with a change in the flow pattern from one with a near-zero boundary condition to one with a substantial wall slip velocity.

Having established the above we shall examine more closely the rheology of the flow within the 'extrusion window' itself ($T \approx 148$–152°C), and specifically identify the contributions of the entry (and exit) and the capillary region to the total pressure drop.

EXPERIMENTAL

Capillary extrusion experiments were performed using a Davenport capillary rheometer (Daventest) described in detail elsewhere[1]. For the studies concerning die geometry, stainless steel capillary dies were employed having capillary lengths and diameters ranging from 2 to 22 mm and 2 to 8 mm, respectively. Several constrictions were employed having entrance angles (2α, whole apex) varying from 30 to 180° (flat entry). An orifice die was used in order to investigate whether the window effects were also prominent in the absence of a capillary wall. This zero-length capillary orifice die consisted of a $2\alpha = 90°$ conical entrance and a 120° exit aperture; the orifice diameter was 2 mm.

Constriction-free extrusion experiments were carried out using the cylindrical reservoir of the rheometer as a capillary. For this purpose a Göttfert Rheograph 2002 viscometer was used. The barrel diameter was 12 mm and the force on the ram was measured as a function of piston displacement. In all but one set of extrusion experiments, a fixed quantity of polymer corresponding to a height of 150 mm in the reservoir was extruded.

Investigations on the influence of die wall material on the extrusion window were conducted at a fixed die geometry and extrusion temperature. A $2\alpha = 90°$ conical entrance and $L/D = 14/2$ capillary was employed and the temperature of extrusion was 150°C. The materials tested included poly(tetrafluoroethylene) (PTFE), stainless steel, phosphor bronze, copper and tungsten carbide, and the tests consisted of a comparison of the stress levels at the onset of the extrusion window (see below).

In all extrusion experiments a linear high molecular weight polyethylene was used (HD6720pr200, supplied by DSM). The intrinsic viscosity, measured in decalin at 135°C, was 4.0 dl g^{-1}. Gel permeation chromatography (g.p.c.) results indicated that the weight average molecular weight M_w was 2.8×10^5 and that the polydispersity M_w/M_n was 7.5. Specimens for extrusion were prepared by powder compaction at ambient temperature and melting of the polymer at 180°C (30 min) to erase the nascent grain structure. Prior to each experiment, the sample was conditioned at the preselected temperature (15 min).

RESULTS

Methodology: p vs. v curves

Continuation of the approach used earlier[1] would involve an analysis through p vs. T curves. Specifically, we would register the critical v (v_c) together with the corresponding p value (p_c) from a series of plots such as in *Figure 1* for each flow field geometry, also defining the T window in the process. Presently, we adopt a different

procedure by which the critical v and p can be determined from a single plot of p vs. tv at a T value corresponding to the location of the T minimum of the window ($T_{min} = 151 \pm 1$ C) in *Figure 1*.

The p vs. v curves (or 'apparent flow curves') are of interest in their own right and will form the subject of the final experimental section of this paper and of the next publication. At this point they are invoked as providing a method for determining critical velocities (apparent wall shear rates) and pressures (apparent stress values). The applicability of this method is based on the fact that the p vs. v curves display a sharp discontinuity within the temperature interval (denoted as T_{in}) defining the T window when the critical v for the window effect is reached, apparent as a sharp drop in the p vs. v curves such as in *Figure 2*. Here the value corresponding to the local maximum preceding the drop identifies the critical piston velocity (v_c) pertaining to the particular die geometry. In fact, v_c thus identified in *Figure 2* closely agrees with the v value at which the appearance of the minimum in the p vs. T trace is first observed in *Figure 1*, both giving $v_c = 1.88 \pm 0.13$ mm min^{-1}. As can be seen, the two methods of registering the onset of the rheological window effect are in quantitative agreement.

Figure 2 should be compared with the more usual p vs. v plots at conventional processing temperatures, i.e. above the T window (*Figure 3*). More of the distinction between *Figures 2* and *3* will be said in our next paper. Here we just note that 'flow curves' such as *Figure 2* can serve to identify the 'window' in terms of T by recording them as a function of T, and subsequently the critical velocity by recording a single p vs. v curve within the temperature interval (T_{in}) of the window thus identified. It is to be noted that the anomalous rheological effect, as displayed by flow curves such as *Figure 2*, pertains over the full T range of the window (T_{in}), and its

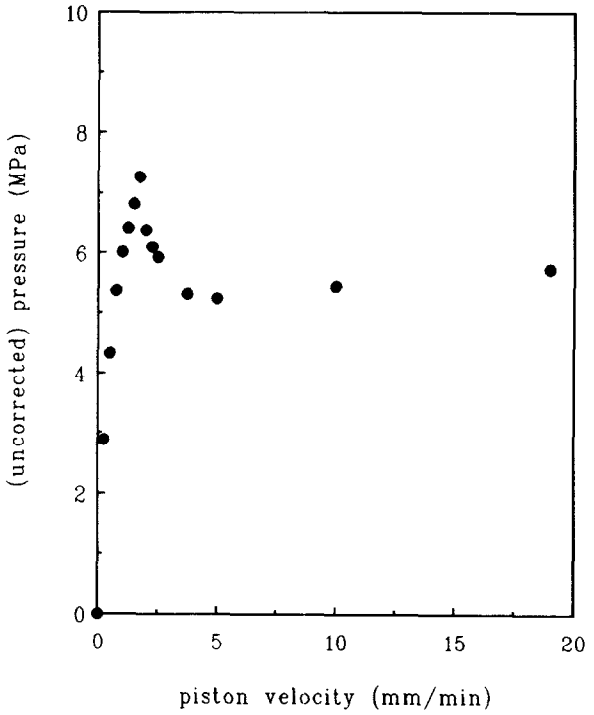

Figure 2 Pressure vs. piston velocity trace ('flow curve') at $T = 151.0$ C (T_{min}) (capillary $L/D = 14.2$, $2\alpha = 90°$)

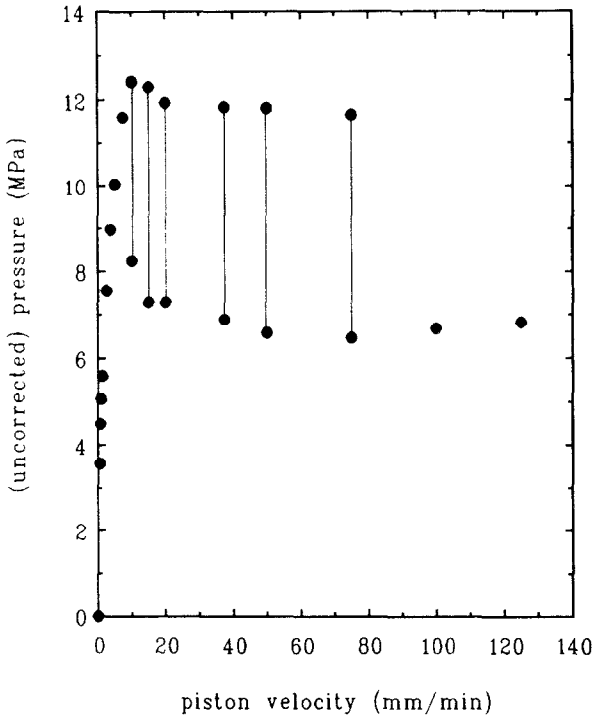

Figure 3 Pressure vs. piston velocity trace at 180 C

appearance at v_c can therefore be used to define the T interval T_{in}, which in the case of *Figure 2* is 148–152°C. The effect is nevertheless most pronounced at the T value (within T_{in}) where p has its sharply defined minimum in *Figure 1*, to be denoted T_{min}. Here we shall use the previously established value of T_{min} from p vs. T traces such as in *Figure 1* (where $T_{min} \approx 150$°C) at which to record p vs. v traces (such as *Figure 2*) as a function of various further variables for the ready identification of the critical velocity and the associated critical pressure level. This isothermal (or 'static') method of diagnosis has certain advantages over the method based on the p vs. T curves in the first part of this series (there termed 'dynamic mode'). Namely, with v being a continuously changing variable (as opposed to showing stepwise increases in recording p vs. T curves such as in *Figure 1*), the determination of v_c is more accurate, while the whole procedure, relying on a single curve, is less time consuming. This simplification itself relies on the previously established knowledge that, to a good approximation, the window minimum temperature (T_{min}) itself is unaffected by v (see *Figure 1*). Another obvious advantage of the 'static' experiment relates to the T_{min} value being independent of the wall material used.

On the presentation of results

In our capillary flow experiments, the primary experimentally determined and measured quantities were the piston velocity (v) and pressure drop (p)*, in terms of which *Figures 1–3* (as indeed all preceding figures in our earlier paper[1]) have been presented. When comparing

* In our discussion we shall use the symbol p to denote pressure drops. Strictly speaking, the measured pressure drop (Δp_{tot}) equals the difference between p and atmospheric pressure p^0 (i.e. $\Delta p_{tot} = p - p^0$). However, as $p^0 \ll p$, we take $\Delta p_{tot} = p$

the effects for different flow geometries, a method of normalizing with respect to the relevant geometrical variables would need adopting. Following standard rheological practice, in principle this can be done by expressing the results in terms of the rheological variables shear rate ($\dot{\gamma}$) and shear stress (τ) in place of v and p, respectively. However, conversion of the directly measured v and p into their respective derivatives $\dot{\gamma}$ and τ relies on a precise knowledge (or assumptions) of the flow field within the capillary die, which, together with the underlying fundamentals, will be laid out in what follows.

Taking pressure first, this will be compounded from the pressure drop over the capillary and from pressure drops arising within the entrance and exit regions (the latter designated collectively as 'end losses'). When changing capillary length only, the end losses are assumed to remain unaffected, which is the basis of the Bagley analysis (see later). As we shall be concerned mostly with effects in the capillary, we express p as the stress exerted on the wall of the capillary, readily derived from the force balance. On the assumption that the axial pressure gradient within the capillary $\partial p/\partial z$ is constant (z being the axial distance in the capillary), the wall shear stress τ_w can be expressed as

$$\tau_w = \frac{\Delta p_{cap}}{4(L/D)} \tag{1}$$

It follows from equation (1) that the capillary pressure drop Δp_{cap} for a given wall stress is inversely dependent on the capillary diameter and proportional to the capillary length. The p value as measured ($\Delta p_{tot} \equiv p$) will contain the contributions due to the ends, and similarly the stress derived therefrom through equation (1). These quantities, based on Δp_{tot}, will be referred to as 'uncorrected pressure' and 'uncorrected wall stress', respectively, in what follows. The correction which allows determination of the portion of the pressure drop pertaining to the capillary alone can be carried out through application of the Bagley analysis mentioned above and to be defined more explicitly further below.

For the influence of v, the effective quantity is the relevant velocity gradient. The situation will clearly be complex within the entry region, with both transverse and longitudinal velocity gradients present. It is the longitudinal velocity gradient which has received most attention in past works on melt flow leading to the solidification effects referred to in the introduction to our earlier paper[1]. For this we shall test again below when changing the entrance geometry.

For the capillary portion, which has become the focus of our present attention, matters greatly simplify. Here, along the central flow axis ($r=0$, where r is the radial distance as taken from the central flow axis) of the capillary the transverse velocity gradient $(\partial u/\partial r)_{r=0} = 0$. At the site of the capillary wall ($r = D/2$), $\partial u/\partial r$ is maximum. When, for a given piston velocity, and hence throughput (Q), the capillary dimensions are varied, the transverse velocity gradient at the capillary wall $(\partial u/\partial r)_{r=D/2}$ will only depend on the diameter of the capillary and will remain unaffected by changes in L. For given capillary dimensions the actual velocity profile is solely determined by the constitutive behaviour of the polymer. For capillary flow an 'apparent wall shear rate'

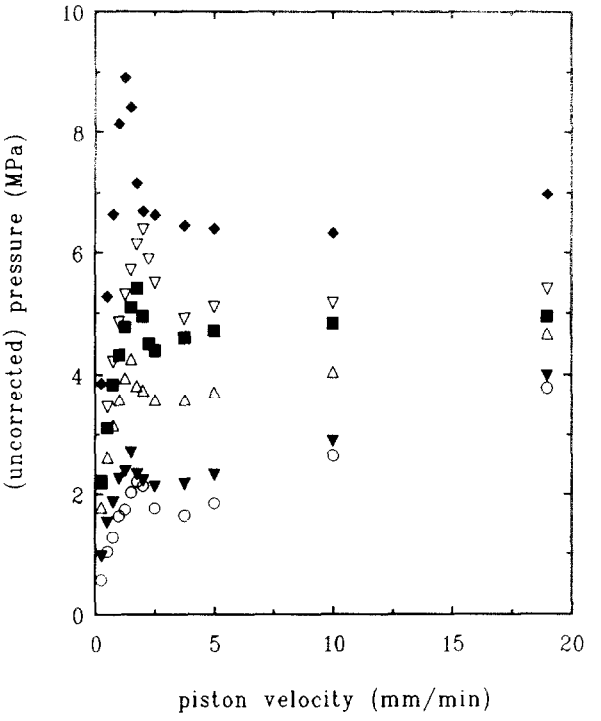

Figure 4 Pressure vs. piston velocity curves obtained for different capillary lengths (L): (○) $L=2$; (▼) $L=4$; (△) $L=8$; (■) $L=10$; (▽) $L=12$; (◆) $L=18$ mm (capillary $D=2$ mm, $2\alpha=90°$)

can be defined as

$$\dot{\gamma}_A = \frac{32Q}{\pi D^3} \tag{2}$$

where the constants pertain to the case of ideal Poiseulle flow, i.e. to a parabolic velocity profile. Since in our case such an idealization of the flow is not assured, we affix the subscript A which stands for 'apparent'.

In what follows we shall express the results in terms of τ_w (the terms 'corrected' and 'uncorrected' will be explicitly included) and $\dot{\gamma}_A$ wherever this is helpful*. These, through the respective equations (1) and (2), relate directly to the primary measured quantities p and v through simple factors of multiplication. These multipliers contain capillary dimensions which allow us to compare the normalized critical values of p and v obtained for different capillary dimensions.

Flow criticalities

Variation of capillary length. In *Figure 4*, p vs. v traces are given for different capillary lengths at a fixed diameter ($D=2$ mm) and entrance angle ($2\alpha=90°$). For all capillary lengths investigated ($L=2$–18 mm), the flow curves are such as in *Figure 2*, i.e. with a usual portion in which $\partial p/\partial v > 0$ followed by an anomalous portion in which the gradient $\partial p/\partial v < 0$, with the sharp maximum where the slope changes sign corresponding to the critical point where the anomalous flow effect in question sets in. At higher values of v, the p vs. v curves level off to a (lower)

*To put into perspective, the apparent shear viscosities of high M polyethylene at 150 C and shear rates of $<10\,s^{-1}$ are of the order of 10^4 Pa s, compared with the target viscosities of <500 Pa s for many commercial extrusion processes

plateau, after which they are seen to bend upwards, the rate of increase of p with v being a decreasing function of L, to be commented on again further below. Using equations (1) and (2), the critical apparent wall shear rate and critical uncorrected wall stress values can be evaluated from the values of v and p at the (local) maxima in the respective curves. In *Figures 5* and *6*, the critical apparent shear rate and uncorrected stress (top curve) at the start of the extrusion window are given as a function

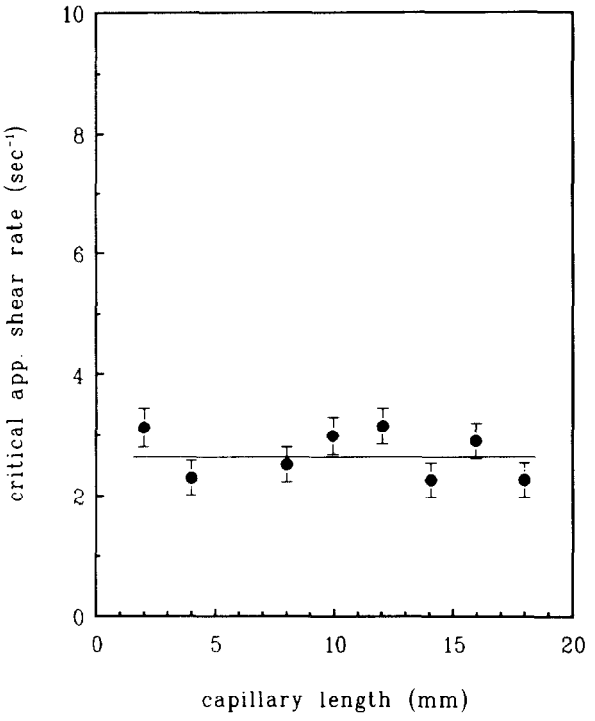

Figure 5 Critical onset apparent wall shear rate ($\dot{\gamma}_{A,c}$) as a function of L (capillary $D = 2$ mm, $2\alpha = 90°$)

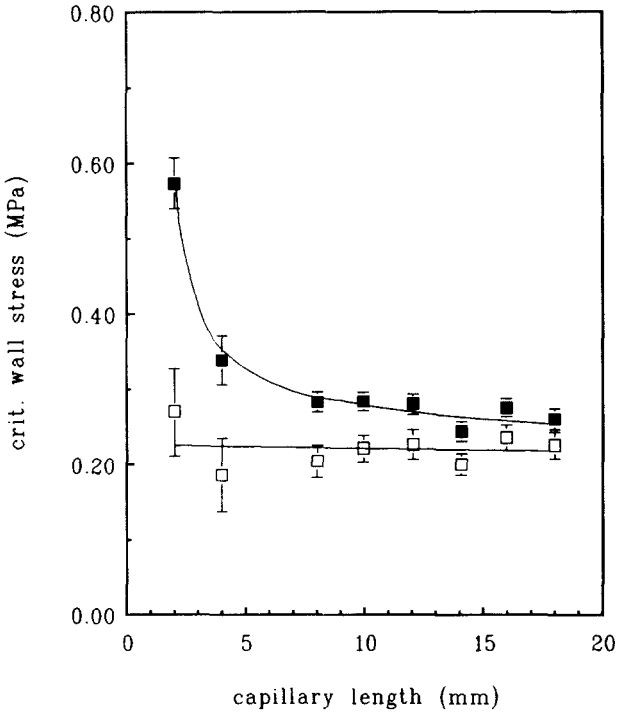

Figure 6 Critical onset uncorrected wall shear stress (■) and corrected wall shear stress (□) as a function of L (capillary $D = 2$ mm, $2\alpha = 90°$)

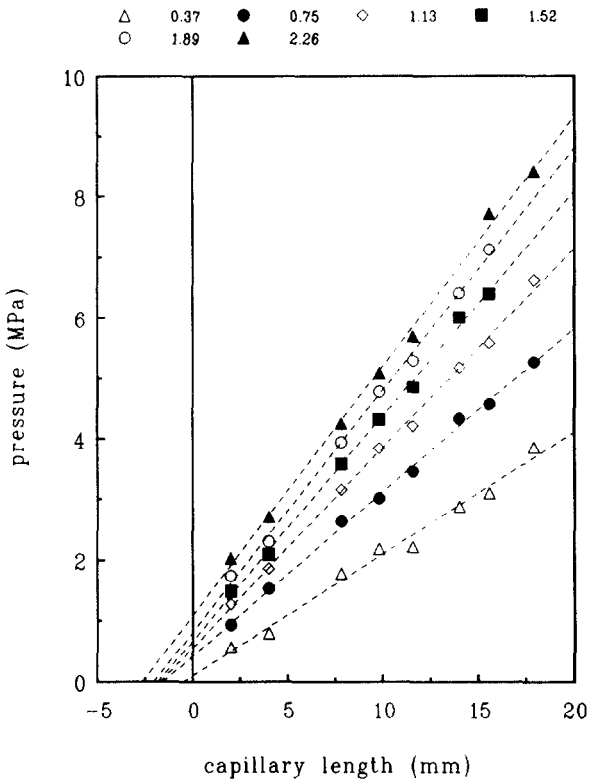

Figure 7 Bagley plots for conditions preceding the extrusion window ($\dot{\gamma}_A < \dot{\gamma}_{A,c}$) at $T = 151.0$°C ($\dot{\gamma}_A$ values in s^{-1} are indicated) (capillary $D = 2$ mm, $2\alpha = 90°$)

of capillary length. It is readily observed from *Figure 5* that the critical apparent shear rate remains unaffected by variations in the capillary length. On the contrary, the uncorrected stress values reported in *Figure 6* decrease with capillary length. The overall pressure drop can be thought of as being composed of three different constituents

$$\Delta p_{tot} = \Delta p_{cap} + \Delta p_{entry} + \Delta p_{exit} \quad (3)$$

In the calculation of the critical wall stress in *Figure 6* (top curve), the pressure drop still contains contributions from the pressure losses at the ends. In order to determine the stress value at the capillary wall, the end losses have to be corrected for. As mentioned previously, this can be done using the Bagley analysis[7], according to which it is assumed that the entry and exit constituents of the total pressure drop remain unaltered when varying L. Thus, when Δp_{tot} is plotted as a function of L, extrapolation to zero capillary length gives the end pressure loss, which is the sum of Δp_{entry} and Δp_{exit}. In *Figure 7* such Bagley plots are depicted for several values of the rate of extrusion up to the critical points of *Figure 4*. All plots in *Figure 7* are linear, in accord with the additivity approximation of capillary and end pressure drops. (From the value of Δp_{ends} for the top plot in *Figure 7*, the end loss at the critical point is calculated to be about 1.09 MPa*.) In the discussion to follow, Δp_{exit} is assumed to be negligible with respect to Δp_{entry}. In the bottom curve of *Figure 6*, the corrected stress values given were

* In conventional rheological practice, the 'ends correction' is usually expressed in terms of the extrapolated intercept on the x axis. In view of the linearity of the Bagley plots (*Figure 7*), our procedure is equivalent

calculated using equations (1) and (3). It is seen that the critical onset corrected wall stress is independent of L.

In *Figures 5* and *6*, the capillary length was varied from 2 to 18 mm. The p vs. $\dot{\gamma}_A$ curve measured for the zero capillary length die (orifice die) at T_{min} is shown in *Figure 8*. This figure demonstrates that p is a monotonically increasing function of $\dot{\gamma}_A$, without any sign of a minimum in p when the capillary part of the die is absent. It follows that the existence of a capillary is necessary for the discontinuity, and hence the anomalous effect of our current interest, to appear.

Variation of capillary diameter. In previous experiments, the capillary diameter was kept fixed with the length being varied. Presently, we shall vary D with L constant. For all capillary bore diameters studied, characteristic flow curves like the ones given in *Figures 2* and *4* were obtained. (For the sake of concise presentation these are not shown.) The apparent wall shear rate at the start of the window, evaluated from the set of flow curves, is shown in *Figure 9* as a function of the reciprocal capillary diameter. Here, the critical onset shear rate is seen to be a slightly decreasing function of the reciprocal diameter, a wider capillary requiring a higher apparent shear rate (and hence throughput) for the singularity to set in. Moreover, when extrapolating to $D^{-1} = d^{-1} = 0.10\,mm^{-1}$ (where d is the reservoir diameter), *Figure 9* suggests that the extrusion window effects could also be obtained in the absence of a constriction, i.e. without the extensional flow component. (For constriction-free flow experiments see below.)

Variation of entrance angle. The strength of the elongational flow can be altered through variation of the entrance angle to the capillary. It can be readily seen

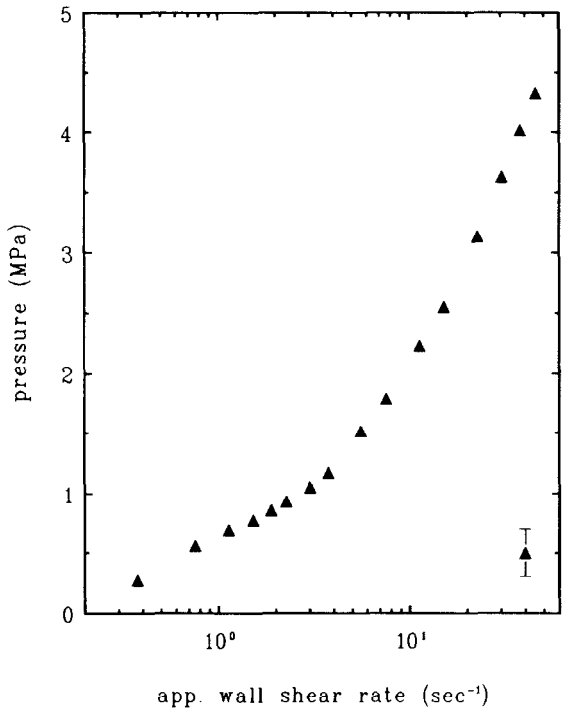

Figure 8 Pressure vs. apparent wall shear rate for an orifice die at $T = 151.0$ C (orifice $L = 0$, $D = 2$ mm, $2\alpha = 90$, exit $2\alpha' = 120$). A typical error bar is indicated

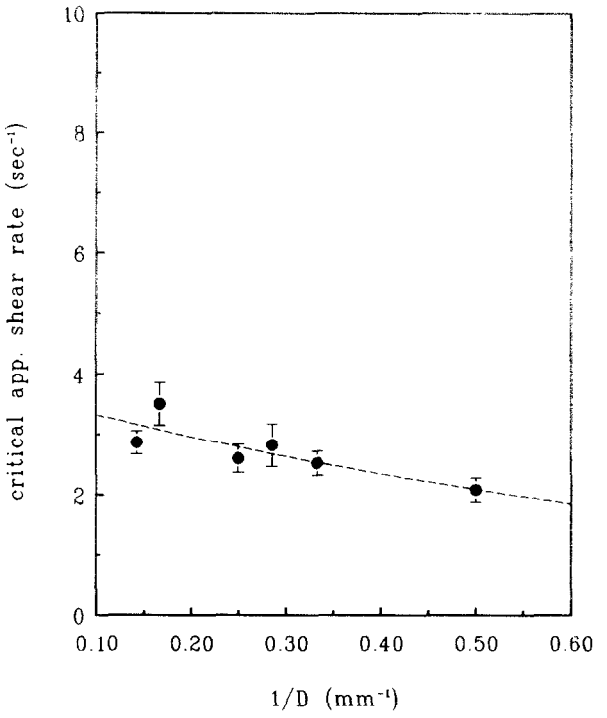

Figure 9 Critical onset apparent wall shear rate vs. reciprocal capillary diameter (capillary $L = 14$ mm, $2\alpha = 90$)

Table 1 Critical apparent wall shear rates at the onset of the extrusion window in high density polyethylene (capillary $L/D = 14.2$, $T = 151.0$ C) and at the onset of flow-induced crystallization effects in i-PP

Entrance angle 2α (°)	Extrusion window $\dot{\gamma}_{A,c}$ (s^{-1})	Crystallization $\dot{\gamma}_{A,c}$ (s^{-1})
0	2.67 ± 0.67^a	–
60	2.08 ± 0.19	1100
90	2.26 ± 0.29	500
120	1.70 ± 0.19	265
180	2.08 ± 0.19	

[a] Obtained from tube flow experiments ($d = 12$ mm) (see text)

even qualitatively that for fixed barrel and capillary diameters, the 'strength' of the elongational flow is expected to increase with increasing entrance angle (2α) owing to the ensuing larger convergence.

The critical onset apparent wall shear rate ($\dot{\gamma}_{A,c}$) for the extrusion window at $T_{min} = 151$ C is contained in *Table 1* for several entrance angles. It is seen from *Table 1* that $\dot{\gamma}_{A,c}$ is insensitive to changes in the geometry of the entrance zone. This is strong support for the view that the entrance, and hence the elongational flow, has little influence on the window effect, which accordingly should have its origin in the capillary. For comparison, *Table 1* also contains the critical apparent wall shear rates for the onset of flow-induced crystallization effects in isotactic polypropylene (i-PP) taken from the first report on such solidification effects by van der Vegt and Smit[6]. As seen, in this case there is a strong dependence of the wall shear rate on 2α, to be commented on further in the Discussion.

In the above extrusion experiments, the entrance angle was varied at fixed capillary dimensions. These experiments were also extended to include variations in

L. The p vs. v curves such as in *Figures 2* and *4* recorded on a series of 90° and 180° dies having different lengths (L ranging from 2 to 22 mm) revealed that the apparent wall shear rate at the start of the extrusion window ($\dot{\gamma}_{A,c} \approx 2.1\ s^{-1}$; see *Table 1*) remained unaffected by variations in either 2α or L. Furthermore, the existence of the extrusion window has also been corroborated using dies of slit geometry ($2\alpha = 90°$, capillary $L \times D \times W = 14 \times 2 \times 2\ mm^3$).

Flow curves

Determination of end losses. So far we have been concerned with flow criticalities, i.e. v_c and p_c or equivalently $\dot{\gamma}_{A,c}$ and $\tau_{w,c}$. Now we turn to the full flow curve such as displayed by *Figures 2* and *4*. Again, varying the capillary length for rates of extrusion up to the respective critical point (v_c) in *Figure 4* (identified with the onset of the extrusion window), the Bagley plots yielded straight lines. The Bagley scheme was also applied for rates above v_c ($\dot{\gamma}_{A,c}$). Here as well it yielded straight p vs. L plots for each value of constant rate. In *Figure 10* the end losses obtained for a range of v (and hence $\dot{\gamma}_A$) encompassing the full flow curve are given as a function of apparent wall shear rate. The end losses in *Figure 10* display two regimes corresponding to flow conditions present prior to the singularity signalling the onset of the window (filled circles) and to conditions pertaining beyond the singularity, i.e. corresponding to the extrusion window itself (open circles). At $\dot{\gamma}_{A,c}$ there is a discontinuity in the Δp_{ends} vs. $\dot{\gamma}_A$ curve which is probably associated with the interaction between the flow field upstream of the die and the one within the capillary when the extrusion window effect sets in, namely the adoption of a different mode of flow pertinent to the extrusion window[8]. The discontinuity at $\dot{\gamma}_{A,c}$ apart, the dominant overall trend is that the end losses are increasing indefinitely with

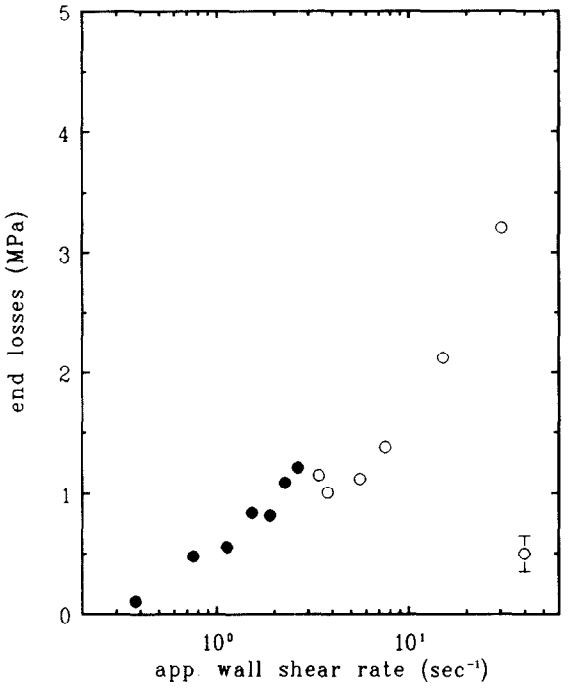

Figure 10 End losses determined according to the Bagley method as a function of apparent wall shear rate at $T_{min} = 151.0°C$: (●) normal flow conditions present prior to the extrusion window effect; (○) conditions pertaining to the extrusion window effect (a typical error bar is indicated)

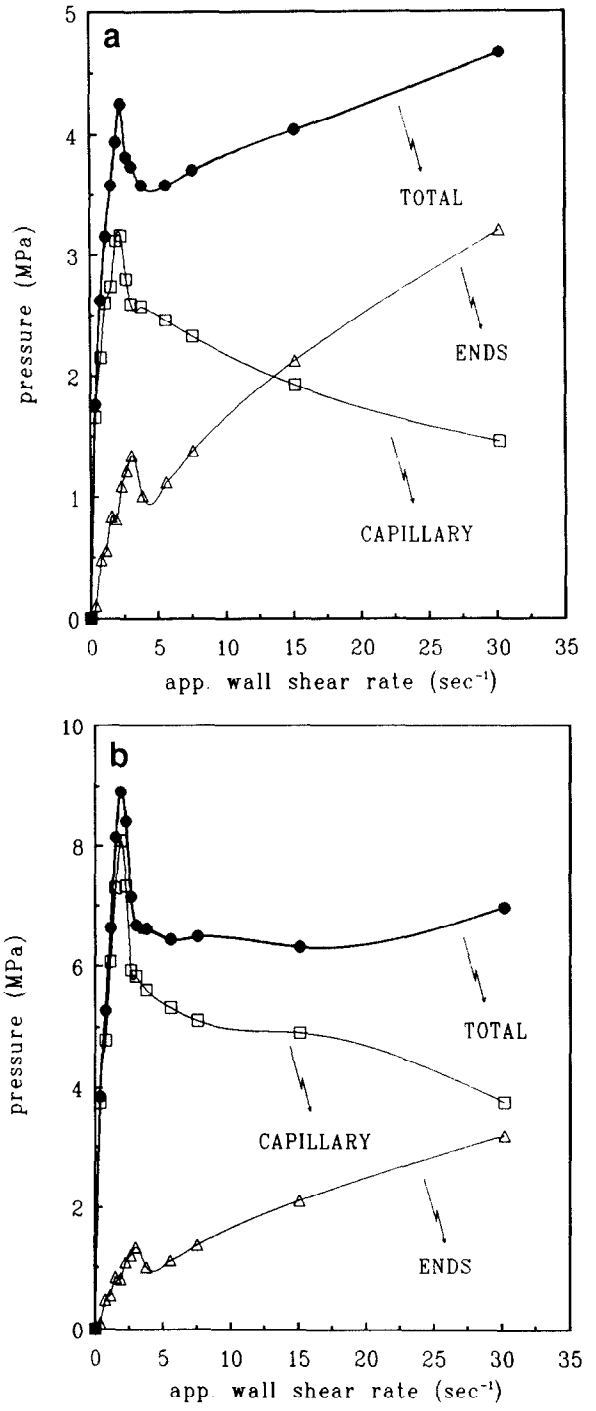

Figure 11 Decomposition of measured total pressure drop (●) into capillary pressure drop (□) and end losses (△) at $T = 151.0°C$ (capillary $D = 2$ mm, $2\alpha = 90°$): (a) $L = 8$ mm; (b) $L = 18$ mm

increasing rate of flow*. This important finding will be referred to later when discussing the role of the entrance and capillary in the extrusion window effect.

Decomposition of total pressure drop into its constituents. Knowing the magnitude of the contributions of the entry and exit losses to the overall pressure drop as a function of $\dot{\gamma}_A$, it is possible to determine the capillary pressure drop for each value of L as defined by equation (3). In *Figures 11a* and *11b*, the decomposition of Δp_{tot} into

* It is noted that qualitatively similar results to *Figure 10* have been obtained by applying the scheme due to Bagley to capillary dies having a flat ($2\alpha = 180°$) entry

Δp_{ends} and Δp_{cap} is shown for capillary dies having $L/D = 8/2$ and $18/2$, respectively. As can be seen, the plot of Δp_{tot} vs. v as measured directly is, beyond v_c (and hence $\dot{\gamma}_{A,c}$), the resultant of a rising Δp_{ends} and a falling Δp_{cap}. It follows that the extrusion window effect, reflected by a sudden decrease in Δp_{tot} beyond $\dot{\gamma}_{A,c}$, is due to a progressive reduction in Δp_{cap}, an effect pertaining to all $\dot{\gamma}_A$ investigated. The upswing in Δp_{tot} at higher rates in *Figure 11a* (and also in *Figures 2* and *4*) is therefore entirely attributable to the rise in Δp_{ends}. Support for this can be found when comparing *Figures 11a* and *11b*. On increasing v, Δp_{ends} will increasingly dominate leading to an eventual rise in Δp_{tot}. For longer L, this rise will be progressively deferred to higher extrusion rates, which, as apparent from *Figure 11b*, can produce a horizontal plateau followed by the rising portion of the $\Delta p_{tot} \equiv p$ vs. v curve, the length of which increases with L.

The flow curve corrected for end losses. When the end losses determined according to the Bagley scheme, shown in *Figure 10*, are applied to all the apparent flow curves pertaining to different L in *Figure 4*, all the 'corrected' flow curves are found to superpose. The master curve thus obtained is depicted in *Figure 12*. It is readily observed from *Figure 12* that above $\dot{\gamma}_{A,c}$ the corrected capillary wall stress decreases monotonously with increasing $\dot{\gamma}_A$, i.e. the throughput, or the rate of decrease $\partial\tau_w/\partial\dot{\gamma}_A$, is a decreasing function of $\dot{\gamma}_A$. Here, we merely remark that above $\dot{\gamma}_A \approx 50\,s^{-1}$ a flow instability sets in causing severe random distortions in the extrudate, which will be the subject of the next paper in this series.

Tube flow experiments. It would follow from all experimental results obtained so far that it should also

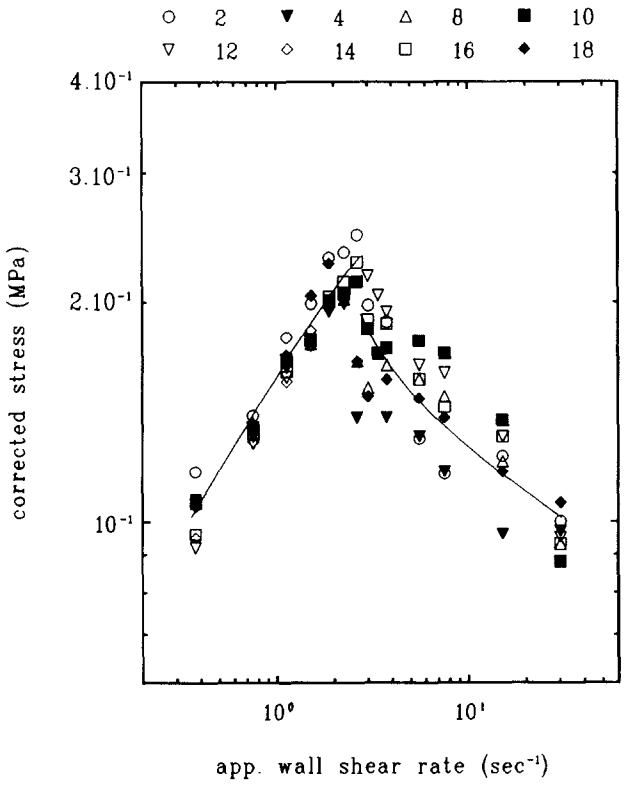

Figure 12 End loss corrected flow curves ('master curve') for capillaries of different length (L) from *Figure 4*. The L values are indicated in the figure ($T = 151.0$°C) (capillary $D = 2$ mm, $2\alpha = 90°$)

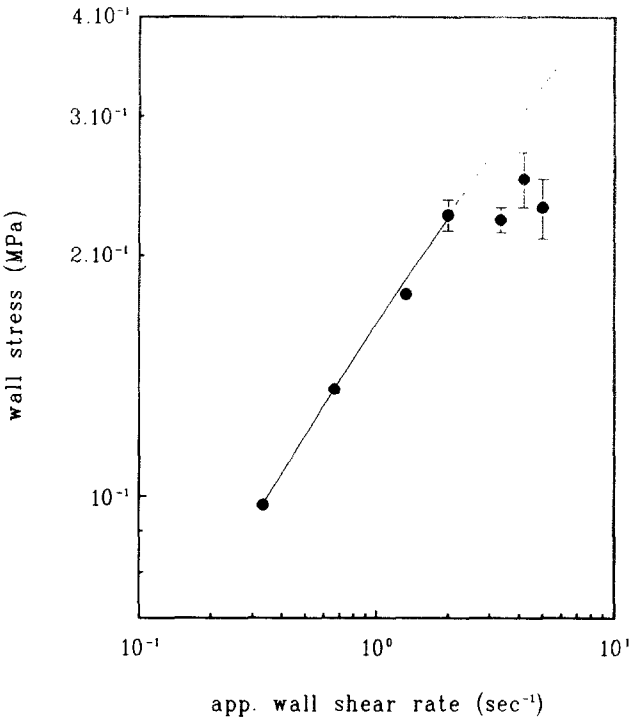

Figure 13 Wall shear stress vs. apparent wall shear rate for tube flow experiments at $T = 150$°C

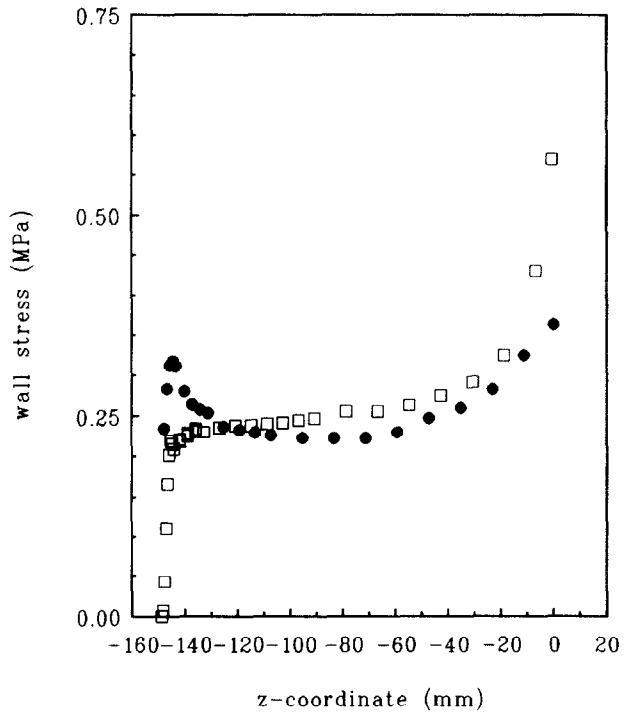

Figure 14 Wall shear stress as a function of axial displacement (z) during tube flow experiments at $T = 160$ C (□) and $T = 150$ C (●)

be possible to find the window effects even without any constriction. The results of constriction-free tube flow extrusion experiments are included in *Figures 13–15*. Plotting the extrusion stress obtained from the force on the piston as a function of apparent shear rate at the wall of the reservoir at the extrusion temperature of 150°C (*Figure 13*) reveals that the flow curve in the absence of a constriction exhibits some of the features characteristic of the (end loss corrected) flow curve related to the

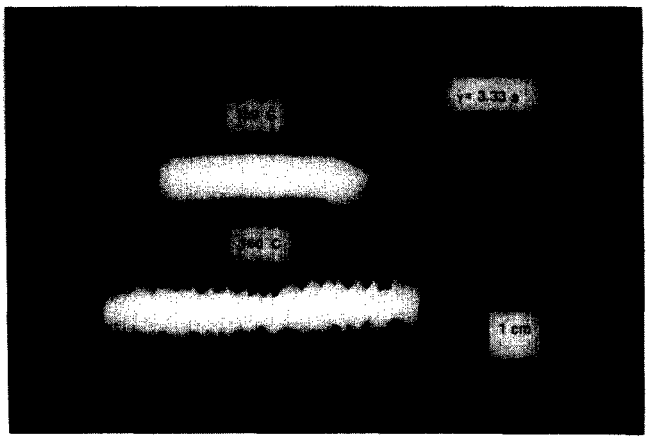

Figure 15 Photograph of extrudates prepared under the conditions in *Figure 14*

extrusion window of *Figure 12*: at the lower rates, a portion is present where τ_w increases with increasing $\dot{\gamma}_A$, which is the expected behaviour. At a certain critical value of $\dot{\gamma}_A$, this increasing trend (denoted by the dashed line in *Figure 13*) is interrupted: now a decrease in τ_w with $\dot{\gamma}_A$ seems to set in. (The highest rate reported in *Figure 13* ($\dot{\gamma}_A \approx 7.5\,s^{-1}$) corresponds to the limit of the apparatus, and hence data at higher $\dot{\gamma}_A$ could not be obtained.) Even the $\dot{\gamma}_A$ value at the end of the increasing trend $\dot{\gamma}_{A,c}$, estimated to be $\sim 2.7 \pm 0.7\,s^{-1}$ from *Figure 13*, is in full accord with the one based on extrapolation of D^{-1} to $D^{-1} = d^{-1}$ in *Figure 9*. Also, it is close to the value of $\sim 2.1 \pm 0.3\,s^{-1}$ obtained when extrapolating to the entrance angle $2\alpha = 0°$ in *Table 1*. We see that full consistency between the flow behaviours in the two systems with and without constriction has been achieved.

In *Figure 14* the wall stress* is plotted as a function of axial displacement (z) (sample height under the ram) for two temperatures of extrusion: the open squares correspond to the temperature of 160°C and the filled circles to 150°C. (The apparent wall shear rate $\dot{\gamma}_A$ in *Figure 14* was $3.3\,s^{-1}$, i.e. corresponding to the portion of the flow curve in *Figure 13* beyond the discontinuity, i.e. the departure from the smooth rising portion.) To take the higher temperature ($T = 160°C$) first, the stress at the wall is first seen to rise steeply when the flow is started. After this initial rise the stress levels off at a value of ~ 0.25 MPa. At the end of the experiment when the reservoir is nearly empty, i.e. when $z \to 0$ in *Figure 14*, the stress rises steeply.

At the lower extrusion temperature of 150°C, i.e. at a temperature corresponding to the temperature window interval, the stress initially rises to a level ($\tau_w \approx 0.33$ MPa) which is considerably higher than the one for 160°C ($\tau_w \approx 0.23$ MPa). Hereafter, the stress decreases with increasing axial piston position, eventually levelling off at a value ($\tau_w \approx 0.22$ MPa) that is lower than the one obtained for the higher extrusion temperature of 160°C (i.e. $\tau_w \approx 0.25$ MPa) – in fact, corresponding to the value beyond the discontinuity in *Figure 13*. The rise in stress as $z \to 0$ is associated with the emptying of the reservoir; it appears less steep at 150°C than at 160°C.

In *Figure 15*, the extruded articles at 150 and 160°C are shown. The smoothness related to the extrusion window is strikingly apparent, even on the comparatively large scale of the tube flow experiment (i.e. a 'capillary' diameter of 12 mm).

The influence of M. All the effects reported so far were established for a single polyethylene sample with $M = 2.8 \times 10^5$. In our earlier paper[1], it was shown that a pressure minimum could be obtained by using the previously described method of recording p vs. T traces at various extrusion rates for all M in the range 10^5–10^6. Presently, we shall employ the method of monitoring p vs. v traces (i.e. τ_w vs. $\dot{\gamma}_A$) at the window temperature for the examination of the effect of M. *Figure 16* should serve as an illustration, showing τ_w vs. $\dot{\gamma}_A$ curves for $M = 2.3 \times 10^5$, 3.4×10^5 and 5.1×10^5 from right to left, respectively. We see that the entire flow curve shifts to lower values of $\dot{\gamma}_A$ when M is increased. This trend itself is in agreement with the inverse M dependence of the strain rate required to stretch out chains established in preceding works. When testing for a quantitative relation by plotting the $\dot{\gamma}_A$ values from *Figure 16* (open circles) against M (on a logarithmic scale in *Figure 17*), we find that the new results fall on the same straight line as that given by the previous data points from our earlier paper[1] (solid circles) defining the previously established power law relationship

$$\dot{\gamma}_{A,c} \propto M^{-4.0} \tag{4}$$

As the results from our earlier paper[1] were obtained from p vs. T curves and the present ones from p vs. v traces, the equivalence of the two procedures is strikingly demonstrated.

We note from *Figure 17* that within the overall fit to equation (4) the recent data point (open circle) for the highest M material is slightly off the straight line. Even

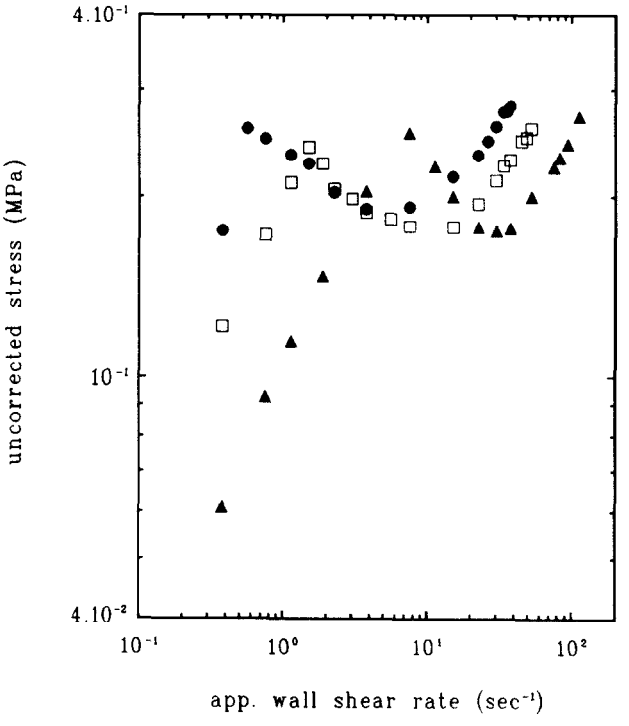

Figure 16 Apparent flow curves at $T = 150.0$ C for several values of molecular weight (M): (▲) $M = 2.3 \times 10^5$; (□) $M = 3.4 \times 10^5$; (●) $M = 5.1 \times 10^5$ (capillary $L/D = 14/2$, $2\alpha = 90°$)

* The wall stress in the tube flow experiment is calculated as the ratio of the piston force (F) and the inner surface area (S) of the barrel: $\tau_w = F/S = F/\pi dz$, where d is the barrel diameter ($d = 12$ mm)

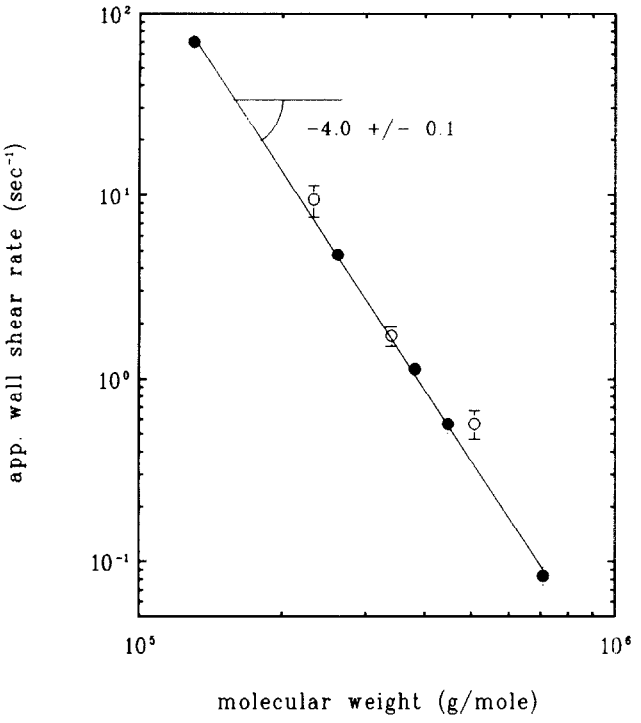

Figure 17 Critical apparent wall shear rate for the onset of the extrusion window vs. molecular weight. The data are from the p vs. T traces of *Figure 1*[1] (●) and from the τ_w vs. $\dot{\gamma}_A$ curves at $T=150.0$°C of *Figure 16* (○) (capillary $L/D=14/2$, $2\alpha=90°$)

this small departure can be accounted for, corroborating rather than detracting from the precise fit to the power law in equation (4) as laid out below.

In our earlier paper[1], T_{min} was shown to shift to slightly higher T with increasing M ($\Delta T \approx 2$–3°C for a decade in M, $M=10^5 \rightarrow 10^6$). The apparent flow curves shown in *Figure 16* were obtained at a single T of 150°C. This corresponds closely to T_{min} for the two materials with the lower M ($M=2.3\times10^5$ and $M=3.4\times10^5$), but is slightly below the exact T_{min} for the polymer with the highest M in *Figure 16* ($M=5.1\times10^5$) (while still being within the limits of the T window of reduced flow resistance). The latter leads to a slightly higher value of $\dot{\gamma}_{A,c}$ as determined at this slightly 'off-minimum' T, which accounts for the upward displacement of the corresponding point from the straight line in *Figure 17*. In fact, the magnitude of this displacement follows nearly quantitatively from the p vs v (and hence τ_w vs. $\dot{\gamma}_A$) plots performed as a function of T throughout this work. While these plots have not been reproduced here in their totality, we present some data at this juncture in *Table 2* for the polymer sample used throughout this paper to illustrate the effect of T on $\dot{\gamma}_{A,c}$ (and on τ_w) in support of the above assertion. We thus see that even what happens to be a minor departure from the $\dot{\gamma}_{A,c}=\text{constant}\times M^{-4.0}$ power law is in fact explicable in terms of the findings presented herein, illustrating the self-consistency of the sum total of the present experimental material.

With regard to the stress values in *Table 2*, it is further observed that the small variation in the uncorrected stress value at the onset of the extrusion window as a function of T is mainly due to the steep increase in Δp_{ends} with falling temperature.

On the role of die wall material

The recording of p vs. v curves for several dies of different wall material yielded apparent flow curves similar to the curves shown in *Figures 2, 4* and *16*. The critical τ_w levels at the onset of the portion of the flow curve where $\partial\tau_w/\partial\dot{\gamma}_A<0$, i.e. at the start of the extrusion window, are given in *Table 3*.

We see that there is a notable difference, well outside experimental error, in $\tau_{w,c}$ for the different wall materials, the lowest value being for PTFE and the highest for tungsten carbide. It follows that the interface, and hence the interaction between the polymer and die surface, has an influence on the effect of our concern. This is consistent with our general assertion, supported by the full body of experimental material presented here, that the origin of the window resides in the vicinity of the capillary wall. More specifically, this result suggests that adhesion between wall and polymer is playing a part in the origin of the window, a point to which we shall return in the following discussion. The sequence itself in *Table 3* may suggest a correlation between $\tau_{w,c}$ and the surface tension of the die material, that being lowest for PTFE ($\gamma \approx 1.3\times10^{-2}$ N m^{-1} at 150°C) and the metals being in the range 1–2 N m^{-1} (for polyethylene at 150°C it has a value around 2.8×10^{-2} N m^{-1})[9].

DISCUSSION

The first paper in this series[1] ended with a complete change in our thinking on the origin of the rheological 'temperature window'. Namely, the invariance of the measured critical pressure (p_c) in the face of a steep (negative fourth power) variation in critical piston velocity with molecular weight (*Figures 12* and *13* in our earlier paper[1]) indicated that the effect corresponds to a yield phenomenon which is likely to be slip along the capillary wall. This is in contrast to the numerous effects associated with the convergence of flow at the capillary entrance, the subject of much previous work. The present results all support the new contention, specificaly that

Table 2 Critical onset apparent wall shear rate, uncorrected wall shear stress, end loss determined using the Bagley scheme and corrected wall shear stress as a function of temperature within the temperature window

Temperature (°C)	$\dot{\gamma}_{A,c}$ (s^{-1})	$\tau_{w,c}^{uncorr}$ (MPa)	Δp_{ends} (MPa)	$\tau_{w,c}^{corr}$ (MPa)
148.0	3.40±0.41	0.320±0.010	1.497±0.08	0.267±0.03
150.0	1.89±0.19	0.245±0.013	0.926±0.05	0.212±0.03
151.0	1.71±0.19	0.222±0.011	0.858±0.05	0.191±0.02

Table 3 Critical (uncorrected) wall shear stress at the onset of the extrusion window for different die wall materials studied ($T=150.0$°C)

Die wall material	$\tau_{w,c}$ (MPa)
PTFE	0.224±0.005
Stainless steel	0.245±0.013
Phosphor bronze	0.258±0.006
Copper	0.287±0.004
Tungsten carbide	0.302±0.005

the source of the 'window' resides within the capillary and not at the orifice, with the concomitant indication that it is associated with effects arising from simple shear flow, pertaining at the confining wall, in contrast to the previously envisaged elongational flow, pertaining at the entry orifice. In this discussion the preceding pieces of evidence will be collated.

First, we remark on the two modes by which the 'window' effect is being recorded. (1) Originally, including its recognition, p vs. T traces were recorded at constant v when the 'window' appeared in a narrow temperature interval (T_{in}) displaying a sharp minimum (T_{min}) at and beyond a critical v (v_c, presently expressed as a critical apparent wall shear rate $\dot{\gamma}_{A,c}$). (2) In much of the present paper, p vs. v traces were recorded at constant T, when the 'window' effect was signalled by a discontinuity in such traces at a specific v (v_c), which only occurred when these traces ('flow curves') were recorded within the narrow temperature region T_{in}. The values of T_{in}, v_c and p_c were identical (or closely similar) in the two kinds of experiment, namely in methods (1) and (2). Thus methods (1) and (2) are mutually consistent, where (2), mainly used in the present paper, has further rheological information to convey (see below).

Support for our revised view that the site of initiation of the 'window' effect is within the capillary (and not the entrance orifice) comes from the following results.

Change in entrance geometry

Change in orifice geometry, specifically the entrance angle (2α), which determines the convergence, and hence governs the 'strength' of the elongational flow, had no effect on the existence and appearance of the 'window', specifically $\dot{\gamma}_{A,c}$ (*Table 1*).

The above results imply that the 'window' effect does not rely on the existence of a constriction at all, and should also arise in a constriction-free, i.e. pure tube flow, experiment. In the present case, this would correspond to flow in the rheometer barrel alone, i.e. without a capillary. While there were certain practical restrictions to such experiments (the wide rheometer barrel at our disposal emptied rather fast for the high piston velocities required), they were sufficiently informative to confirm that this indeed is the case (*Figures 13–15*).

A further implication is that the existence of the capillary is a requirement for the window effect. Again, this could be confirmed: an orifice alone, without a capillary ('orifice die'), did not show the window effect at all (*Figure 8*).

All the above is in contrast to the whole body of previously reported effects (e.g. blockage[6,10,11] formation of special shish kebab based morphologies[12–17]) observed at temperatures which were somewhat below the presently recognized window. Such effects are attributable to flow-induced crystallization, itself due to flow-induced chain extension as produced by elongational flow, and sensitively respond to variations in entrance geometry (the entrance angle α in particular) in agreement with expectations which rely on elongation flow as the source of the phenomenon. The variations in $\dot{\gamma}_{CRIT}$ with 2α for polypropylene, the first material studied in this respect elsewhere[6] ($\dot{\gamma}_{CRIT}$ here meaning the sharp onset of 'shear thickening' rapidly leading to blockage of the flow (see *Figure 3* in our earlier paper[1])), are included in *Table 1*. We see that these variations are pronounced and, as explained elsewhere[6], relate qualitatively to the strength of the elongational flow. Specifically, recalling the work of van der Vegt and Smit[6], the critical apparent elongational flow rate at the orifice ($\dot{\varepsilon}_{A,c}$) is related to the apparent wall shear rate ($\dot{\gamma}_{A,c}$) in the capillary according to

$$\dot{\varepsilon}_{A,c} = K\dot{\gamma}_{A,c} \tan 2\alpha \qquad (5)$$

where K is a constant. The widely varying values of $\dot{\gamma}_{A,c}$ in the third column of *Table 1* correspond to $\dot{\varepsilon}_{A,c}$ remaining constant for a wide range of 2α, in quantitative agreement with the expectation that the blocking, and hence crystallization, effect is induced by elongational flow. It follows, therefore, that the two effects, the previously widely explored flow-induced crystallization and our present rheological window effect, are of different origin. The former is located at the entrance orifice and the latter is within the capillary. Whether any connection exists between the two, and if so what form this takes, is an obvious question to raise (see also our earlier paper[1]) but will not be pursued further here.

We see that the above evidence, even on its own, fully establishes the points in question. Even so, we proceed to invoke additional supporting evidence, both because it strengthens the case further and because each effect is of some interest in its own right.

Change in capillary geometry

Changing length (L) *with diameter* (D) *constant.* Here the first conspicuous effect is the constancy of v_c (*Figure 5*). This in itself is explicable in either way, i.e. by the source of the window effect being in the orifice (i.e. it has no connection with the capillary) or that it is associated with a critical wall shear rate (i.e. $\dot{\gamma}_{A,c}$), which means that it is associated with the capillary itself. These alternatives can be conclusively distinguished by the response of the critical p (p_c) to changes in L. When referred to unit length of capillary, this normalized p_c becomes invariant with L (thus taking on the meaning of wall shear stress τ_w) after correction for end losses (*Figure 6*). This corroborates the contention that the window effect (within the T_{in} range) occurs at a critical stress level, which in the case of the capillary alone (end corrections having been applied) corresponds to a critical capillary wall shear stress ($\tau_{w,c}$).

Looking at it from the point of view of end corrections, all the departures from the invariance of the normalized p_c (and hence uncorrected $\tau_{w,c}$) with changes in L are entirely due to the pressure drops at the orifices – essentially the one at the entrance in the present case. This finding indicates, even at this stage confined to a single rate of shear $\dot{\gamma}_{A,c}$, that the rheological behaviour at T_{in} in the entrance and the behaviour in the capillary are clearly distinct and neatly separable, a line we shall pursue further in the analysis of the flow curves.

Changing diameter (D) *with length* (L) *constant.* The value of D has some effect on $\dot{\gamma}_{A,c}$ in the sense that $\dot{\gamma}_{A,c}$ is larger for larger D (*Figure 9*). This means that a higher rate of shear is required for a wider capillary, which for a constant D means a smaller cross-sectional surface area reduction ratio and hence weaker elongational flow. This itself appears to be in the direction that elongational flow in the orifice is responsible for the window effect.

However, this dependence on D is too small for such an effect to be significant, if present at all. It is more likely that the decrease in $\dot{\gamma}_{A,c}$ with D is associated with a change in the velocity profile within the capillary when varying D (in contrast to varying L when the velocity profile in fully developed flow is expected to remain unaltered). But more significantly, the plot of $\dot{\gamma}_{A,c}$ vs. $1/D$ can be extrapolated to a D value corresponding to the barrel diameter ($d = 10$ mm), i.e. to a situation with no constriction ($D = d = 10$ mm). This corresponds to the situation of our 'tube flow' experiment. As already stated, this extrapolated value for $\dot{\gamma}_{A,c}$ ($3.2\ s^{-1}$) is reasonably close to the one actually determined in our tube flow experiment ($\dot{\gamma}_{A,c} \approx 2.67 \pm 0.67$, see also *Table 1*) as arrived at from *Figure 13*), in satisfactory consistency between the underlying two sets of experiments*.

Experiments on the variation of L (or D) at a fixed L/D ratio revealed that the situation could be treated as the sum total of the experiments described in this section on change in capillary geometry, i.e. all capillaries yielded the characteristic flow curves such as in *Figures 2* and *4*. The $\dot{\gamma}_{A,c}$ value is again a slightly decreasing function of D, which means that a lower $\dot{\gamma}_{A,c}$ is required for a narrower capillary, even for identical L/D ratios, in full accord with the above.

Flow curves

The highly unusual rheological behaviour in the T window is apparent from the p vs. v curves of *Figures 2* and *4* (flow curves) when compared with the conventional behaviour of the same (rather high M) material at higher temperatures corresponding to traditional processing (*Figure 3*). We see that for low v (and hence $\dot{\gamma}_A$), the p vs. v curves rise, first linearly, and then start to level off slightly (shear thinning). Normally, this pattern is only terminated by flow irregularities setting in at some v (and hence $\dot{\gamma}_A$) value which, as in *Figure 3*, is comparatively low. By general experience, this limiting shear rate shifts to increasingly lower values for higher M, setting a limit to practical processability. Even within the smooth portion of the p vs. v (and hence $\dot{\gamma}_A$) trace, the extrudate develops surface roughness ('shark skin') in the higher $\dot{\gamma}_A$ range, making the product itself unsuitable for normal use and thus restricting the extrusion rate applicable in practice still further. (More will be said about product irregularities in our next paper in this series.) In contrast, within the T window the p vs. v trace remains steady, even if it becomes unusual, and the emerging product stays smooth and regular up to very high v (and hence $\dot{\gamma}_A$). (For flow curves extended to still higher $\dot{\gamma}_A$ see the next paper in this series.) Thus extrusion in the T window should have the following advantages: (1) for fundamental enquiries, it enables the extension of meaningful rheological studies over a wider range of flow rates than possible hitherto; and (2) in practice, it should enable faster throughput (and this at lowered energy consumption) in the melt fabrication of such products as lend themselves to this kind of processing.

The unusual nature of the more extended p vs. v curve in the T window has already been referred to (*Figures 2* and *4*). The curve displays a sharp maximum at a kind of singular point which defines v_c and p_c. This is followed by a steep drop leading to a (lower) plateau where the flow resistance (p) remains constant despite increasing v (and hence also increasing material throughput). This plateau, the length of which is an increasing function of capillary length (L), goes over into a renewed rise in p on further increase in v.

For the present, the most significant point is the decomposition of the 'flow curves' into 'end' and 'capillary' components, which amounts to the separation of the pressure drops which occur at the ends (Δp_{ends}), mostly at the entrance, from those over the capillary (Δp_{cap}). This has been described and discussed earlier (*Figures 10*, *11a* and *11b*). Here, we make some additional points or add some special emphasis to these results.

It is of interest to note that the Bagley approach of separation applies even to the present situation along the full 'flow curves'. Specifically, the p vs. L plots give straight lines, and hence allow a meaningful extrapolation to $L = 0$, even for extrusion rates which are beyond the 'critical' point where the flow curves have widely different shapes for different L values.

For the decomposition itself, the first point to note is that both end and capillary contributions display a discontinuity at $\dot{\gamma}_{A,c}$ (*Figures 11a* and *11b*). This on its own may seem to indicate that both sections of the flow field contribute to the window effect. As, however, all the foregoing results decisively speak for the capillary as the site of the effect, it is more likely that the discontinuity associated with the capillary portion of the pressure is the primary effect which then interacts upstream with the flow field in the entrance orifice, as remarked earlier in connection with *Figures 9* and *10*.

Probably more significant than the similarities between Δp_{ends} and Δp_{cap} are the differences between the two: namely that beyond $\dot{\gamma}_{A,c}$, Δp_{ends} rises and Δp_{cap} drops. The plateau in Δp_{tot}, the quantity recorded directly, is therefore the resultant of the two with the plateau (or at least nearly horizontal portion of Δp_{tot}) widening and the upswing shifting to higher $\dot{\gamma}_A$ with increasing L (*Figures 11a* and *11b*). If this trend continued, it should follow that for capillaries still longer than used at present, Δp_{tot} (like Δp_{cap}) will actually become a decreasing function of $\dot{\gamma}_A$, i.e. the 'plateau' will no longer be horizontal but slope downwards over all the practicable flow rates. This would have the consequence that increasing material throughput could be achieved with decreasing input of energy. The intriguing possibility of such a runaway effect, which has come to our notice after completion of the present experimental programme, clearly invites testing.

At this point, possible interpretations in terms of viscosity merit mention. The concept of shear viscosity (η) is in the present case of capillary flow, where the boundary conditions are not established *a priori*, of questionable usefulness. Conventionally, it is a single-constant parameter characterizing the flow behaviour of a particular fluid. In the case of non-Newtonian polymer melts, this uniqueness is clearly being put to the test by its shear rate dependence, leading to concepts such as shear thinning and shear thickening. In the present

* Ideally, of course, the tube should be very long in order to establish fully developed shear flow conditions. As seen from *Figure 14*, when the tube is nearly empty, strong end effects become apparent, which for infinite tube length would be absent. Nevertheless, the tube flow results presented in *Figures 13–15* fully support the contention that happenings in the capillary alone are responsible for the window effect

instance of flow behaviour in the T window, the directly measured quantity, i.e. the pressure drop, is a complex function of the apparent shear rate. Here, the conventional definition of η, when derived from the ratio of end-corrected shear stress to apparent shear rate taken at each $\dot{\gamma}_A$, would give a complex sequence of rising and falling η values, representing little more than a poor substitute for the p vs. t traces themselves. It would be more appropriate to take the slope as defining η (instantaneous viscosity). However, in the present case this would lead to such conceptual problems as negative η values. On the whole, therefore, we feel that nothing would be gained, only confusion created, by invoking viscosity values to express our results based on macroscopic measurements (like p and v) alone. In simpler non-Newtonian melt behaviour, extrapolation to zero shear rate viscosity is resorted to for a single-parameter representation of a fluid and for its evaluation in physical terms. It is readily seen that in the present case within the T window, such an extrapolation would be either meaningless or, if confined to the initial $\dot{\gamma}_A$ range, uninformative, avoiding the effect of real interest.

Interpretation on the macroscopic (flow field) level: shear flow vs. slip

As already stated, macroscopically the T window effect is most readily interpretable as slip, i.e. plug flow setting in for a particular shear stress at the window temperature. Clearly, it would be desirable to map out the flow field itself, both to confirm and to analyse this situation further. Some preliminary observations made in this direction were not sufficiently conclusive, indicating the need for a new programme of work specifically directed to this purpose. Therefore, short of direct visualization, we shall rely on the extensive rheological material here presented to envisage the kind of flows involved. For added confidence, we wish to emphasize the complete self-consistency of all the effects here reported. This is apparent from the experimental results not only in terms of overall trends, but even down to small quantitative details (e.g. extrapolation of the experiments underlying *Figure 9* and the data in *Table 2*, or the correspondence between the present *Figure 17* and *Figure 11* from our earlier paper[1], including the deviation of one point from the exact straight line, etc.).

Prior to the onset of the window, the flow field is expected to have predominantly simple shear character. This means that the velocity of the fluid at the wall will be essentially zero, or very small. Most determinations of rheological properties (e.g. viscosity) rely on such a zero wall slip condition. Once the conditions of the extrusion window are present, i.e. when p is falling with $\dot{\gamma}_A$, all experimental evidence presented above suggests that slip takes place along the capillary wall. *Figure 18* should serve to illustrate the window effect in terms of the flow field. In principle, slippage may be regarded as either 'pure wall slip', which is the case when the fluid moves with a certain velocity (u_{slip}) along the wall (*Figure 18a*), or a 'slip film', where a layer of finite thickness (δ) forms close to the wall with a much reduced viscosity with respect to the bulk. When δ is small with respect to the dimension of the flow channel ($\delta/D \ll 1$), the mathematical treatment of the flow problem is identical to that of 'pure slip'. As will be shown below, the present observations make a strong argument for the case of a 'slip film' as depicted in *Figure 18b*.

Interpretation on the molecular level: flow-induced phase transition along the walls

The essential issues have already been laid out in our earlier paper[1] and will be briefly reiterated for self-contained reading, with the addition of some essential new facts and arguments.

The new rheological window effect is now firmly established from several angles. It consists of reduced flow resistance within a narrow (3–4°C) temperature interval (T_{in}) subject to a critical (apparent) shear rate ($\dot{\gamma}_{A,c}$), itself a sharply decreasing function of molecular

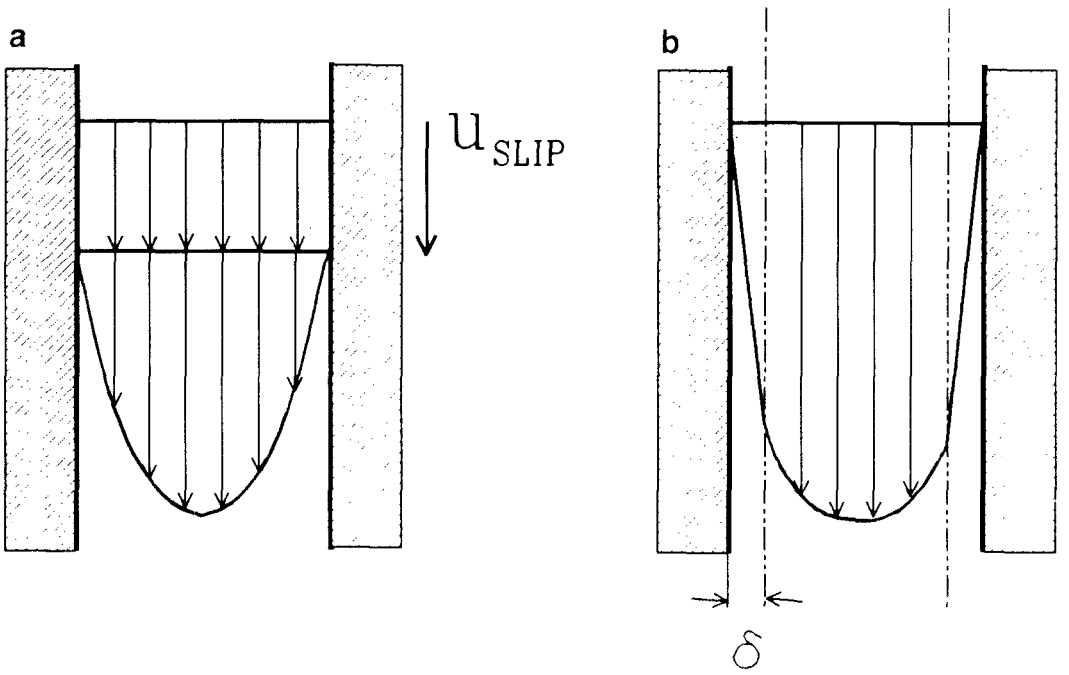

Figure 18 Schematic illustrations of polymer slip along a solid boundary: (a) 'pure wall slip'; (b) 'slip film'

weight, obeying precisely the relation $\dot{\gamma}_{A,c} \propto M^{-4.0}$ (commented on further in our earlier paper[1]). The critical pressure p_c which generates $\dot{\gamma}_{A,c}$ and relates to a critical wall shear stress ($\tau_{w,c}$) within the capillary is strictly constant over the wide M (and hence $\dot{\gamma}_A$) range examined. From this follows, amongst others, that the site of the effect is along the capillary wall and not, as previously envisaged, in the entry orifice. A lead to this conclusion has been provided by our earlier paper[1], fully substantiated from several angles by the various results in the present paper.

The above factual background, and specifically the sharp T dependence of flow resistance, implies that the rheological discontinuity must be of thermodynamic origin, in particular a phase transition. In order to account for the change from predominant shear flow to predominant plug flow, this phase transition must take place at or near the capillary wall in conformity with the rest of the material presented in this paper.

At this point we include a new piece of information which is part of a separate piece of work to be documented elsewhere[18], but nevertheless invited by the present discussion. *In situ* wide angle X-ray experiments carried out on the DASY synchrotron X-ray source in Hamburg (in association with Zachmann) conclusively demonstrated that a phase transition, indicated by the appearance of a crystal reflection located within the capillary portion of the flow field, is indeed associated with the presence of the rheological window.

With regard to the origin of the phase transition, this must clearly be flow generated as signalled by its strong dependence on flow rate (i.e. $\dot{\gamma}_A$). This, together with the criticality observed, points to chain extension as the determining factor on the molecular level, which then would induce a phase transition at the appropriate temperature.

In view of the foregoing results, the chain extension and the ensuing phase transition would need to be at or near the capillary wall. As discussed earlier[1], this at first sight may seem unlikely because near the confining boundary simple shear flow (as opposed to elongational flow at the entry) would dominate, which by *a priori* consideration should not extend chains significantly. However, chain extension could occur if molecules were anchored at the walls, as in the case of adsorption. As already mentioned in our earlier paper[1], melt flow in the presence of adsorbed molecules has been considered theoretically in recent works by Brochard-Wyart and de Gennes[19], who predicted that such flow involves a criticality in shear stress associated with extension of the tube containing the chain molecule (their 'marginal state') at the interface between a surface layer and the bulk melt. Quite recent experimental work by Migler *et al.*[20] using carefully prepared silanated silica surfaces containing adsorbed polydimethylsiloxane molecules established the existence of a sharp transition towards strong slippage occurring within the first 100 nm from the interface, consistent with the above-mentioned theoretical treatment. While a precise connection between the above theoretical and experimental works and our own observations cannot be specified at this stage, it is clear that chain extension along walls, together with the associated criticalities, can be a justifiable proposition*.

Next, we may enquire about the nature of the new phase generated by the phase transition. Again, this topic has featured previously[1]. Briefly, chain extension is expected to raise the melting point, and hence crystallization becomes an obvious possibility. However, it is not obvious why straightforward crystallization should facilitate and not hinder flow (as indeed we know from experiments reported elsewhere[6,10,11] that crystallization can block flow). As is well known, polyethylene can also exist in a mesophase crystal form, intermediate between the usual orthorhombic crystal (o) and the melt, in which the chains are highly mobile. This hexagonal (h) mesophase is metastable under ambient pressures and in the stationary state, but it can become the stable form with a melting point (T_m) higher than that of the orthorhombic form under high pressures or in the constrained extended chain state[22,23]. (In the latter case, chain extension raises $(T_m)_h$ faster than $(T_m)_o$, so that the former can exceed the latter.) A layer of such a 'mobile' h phase along the capillary wall may well account for the reduced flow resistance, particularly when ('near-wall') slip is the determining factor (this situation is depicted in *Figure 18b*). Strong support for this is the apparent uniqueness of the window temperature. Normal crystallization in a polymer requires substantial supercooling, and the exact temperature where crystallization takes place on cooling is neither sharp nor uniquely defined as it strongly depends on the cooling rate. This is in contrast to liquid crystal polymers, where the 'formation' temperature is closely identical to the thermodynamically defined isotropization temperature (T_i) and is hardly affected by cooling conditions. The hexagonal phase in polyethylene is in this respect closer, if not identical, to what could be termed a liquid crystal. In fact, as already stated[1], the window minimum temperature itself (i.e. $T_{min} \approx 150 \pm 1$ C) is closely identical to the o h transition temperature as found in different works elsewhere[22,23].

The most recent *in situ* X-ray evidence using the synchrotron source should in principle provide the keenly awaited answer to the above question. While conclusively confirming that a phase transition is indeed involved, it remains inconclusive with regard to the nature of the newly formed phase. As to be reported separately[18], a single weak X-ray reflection appears simultaneously with the rheological window effect. Such would be expected for the hexagonal phase, but in the case of a rather weak signal this could also be the strongest reflection (i.e. 110) of the orthorhombic phase with the weaker 200 reflection remaining undetected. Of course, in principle the spacing value should be decisive, but the spacing values being very close, the distinction under the present circumstances is marginal. More of this will be discussed in the appropriate publication[18]. Here, it suffices to say that the phase transition itself has been confirmed but the weak single reflection observed is not sufficient in itself to identify the nature of the new phase formed with full confidence. It does, however, follow that the anomalies observed on a macroscopic (i.e. rheological) level must be due to the presence of merely a minute

* Although the theoretical approach pursued by Brochard-Wyart and de Gennes applies to the special case of a 'weak brush' in the limit of a so-called 'mushroom' regime for a monodisperse polymer melt, i.e. it is assumed that adsorbed molecules are entangled with the bulk only and hence do not overlap among themselves, there are recent indications that a similar approach may also be applicable to the case of a polydisperse adsorbed polymer[21]

amount of the newly formed phase, locally arising at or near the capillary wall.

In the light of the above, the previously puzzling observation of the conditional reversibility of the window effect on cooling now seems to fall readily into place, and in fact provides support to the assertions. To recall, it has been found elsewhere[3] that on cooling (and on cooling only) the presence of the 'dip' in the p vs. T curves (such as in *Figure 1*), i.e. the window effect itself, was affected by the pretreatment history. Once the dip had appeared in a heating run it was assuredly present also on immediate cooling, but its appearance became unpredictable after prolonged holding at the elevated temperature at which the heating run was terminated (~ 170°C). Also as found earlier[1], on repeating the runs the p minimum became more pronounced. All this indicates[3] that a variable memory effect of the then-hypothesized newly formed phase is at play. Specifically, the phase transition needs to be nucleated and therefore will be much influenced by pre-existing nuclei remaining in the melt. This effect is more apparent on cooling, i.e. when the transformation temperature is approached from above. Clearly, in a flowing melt with constant material renewal, the residual nuclei must somehow be retained so that they are able to promote the phase transformation within the newly arriving material. In the other work[3], adhesion to the wall was invoked which did not readily fit into the picture of an elongational flow induced phase transformation in the orifice (and, by implication, along the central flow line) – the view held at that time. It is seen that the revised view, namely that the site of action is along the capillary wall, removes the aforementioned conflict. In fact, the requirement of nuclei persisting at the wall corroborates the new picture on the origin of the window effect.

In the above context a further point is of relevance and deserves special emphasis accordingly. In any conventional crystallization on cooling, the temperature range of the phase transition is sensitively affected by the number of pre-existing nuclei. In the dynamic situation in question, an increasing number of nuclei should shift the temperature range of the phase transformation to higher temperatures (and hence lower supercoolings) and vice versa. This is not what is observed in connection with the aforementioned memory effect, which otherwise required the invoking of pre-existing residual nuclei. Namely, the position of the p minimum (along the T axis) remained invariant but the strength of the effect varied within wide limits with prehistory. While contrary to expectations from conventional crystallization, this behaviour would be fully consistent with liquid crystal formation, where supercooling effects are minimal. The hypothesized hexagonal phase in polyethylene would conform to this pattern of behaviour already raised previously.

Wider issues

Interesting as it is in its own right, the extrusion window effect may well be regarded as a rather special phenomenon with relevance limited to special systems under rather circumscribed conditions. To counteract such an impression, we draw attention to the wider issues, of which the present effect may be a special manifestation, with pointers to future developments.

First, there is the polymer melt flow itself. Here, the general issue is the new focus on happenings at the wall, which, as recognized by Brochard-Wyart and de Gennes[19], can be vital factors in determining the nature of the flow itself. Our present findings certainly fit into this newly opened framework. While starting from experimental observations on macroscopic flow behaviour, we arrive at inferences which mesh with the new theoretical approaches starting from molecular considerations and are focused on the nature and the behaviour of the polymer chain at the solid–liquid interface. From the more general standpoint, we may regard a special effect such as the present phase transition as a useful aid. Namely, it serves to illuminate the underlying generalities through enhancing these effects, resulting in highly conspicuous consequences by which they can be readily recognized, appreciated and possibly even utilized.

The above-mentioned theoretical considerations involve adsorption, pointing to the importance of the interaction between a polymer molecule and the confining wall. The latter is also brought out in the present work through the influence of the wall material on the critical onset shear rate of the window effect. It would follow from the results (*Table 3*) that the adhesion between polyethylene and the wall material is strongest for the carbide, weakest for PTFE with the metals in between. This adhesion, even if possibly also influenced by the surface topology (i.e. degree of roughness), should be an indicator of the ability of the solid to anchor the polyethylene molecule, and hence of the strength of adsorption. It is worth mentioning that a similar order of increasing stress levels for some of the materials listed in *Table 3* has been achieved by White *et al.*[24] using biconical rotors to measure viscosities for a styrene–butadiene–styrene rubber compound.

In the context of adhesion, we recall previous observations on the pronounced influence of adhesion on the rheological behaviour of solutions originating from this laboratory[25–28]. It was found that for very high M materials (polyethylene[25,27] and also atactic poly(methyl methacrylate) (a-PMMA)[26–28]) the viscosity, as measured mainly by the Couette method[25–27] but in some instances also by capillary viscometers[27], displayed highly irregular behaviour which could be directly associated with thick polymer layer formation along the rotor surface (which we termed the adsorption entanglement layer[25]). The effect with the more extensively studied a-PMMA in particular turned out to be more complex (and even more interesting), as flow-induced liquid–liquid separation[28], localized along the rotor surface, was found to be involved, but nevertheless with adsorption still as the initiating feature. It is most noteworthy in the present context that the rotor material has a strong influence on the whole group of effects[27]: the largest effect was with carbon, the smallest with PTFE, and various metals were in between. We see that the sequence is the same as in *Table 3* for the present melt flow experiments (with carbon instead of the carbide), underlining the generality of the phenomena involved, specifically the importance of the polymer–wall interaction in the flow behaviour of the polymer system. Combined scrutiny of our experiences with both solutions and melts is clearly invited. This should also include our past experience (preceding the present work) with the rheology of a melt, where a flow gap width dependence was

observed in the flow resistance of atactic polystyrene melts as measured using a parallel plate viscometer[29]. Here, the effect observed differed from that initially expected from an 'adsorption entanglement layer', i.e. the normalized flow resistance (i.e. 'viscosity') was a decreasing function of the gap width below a certain gap width. Whatever the explanation, the effect of a finite boundary layer or some effect associated with polymer–wall contact is indicated, either of which falls within the wider field of interest generated by the present study.

Of course, the interaction between a polymer and the solid surface of another material has consequences beyond melt flow (or solution flow). It is of direct consequence, amongst others, to the friction between two moving solids in contact, where at least one is a polymer. The possibility of chain alignment arises, whether cold or through the intermediacy of local melting. In the latter case, one may count on the subsequent formation of chain-aligned 'mobile' mesophases with a potentially profound influence on frictional properties.

Finally, a remark on the 'flow curves'. Even if very special situations (i.e. shear rate dependence of shear stress within the very narrow T region of the 'window' singularity), they too have more general messages to convey. In view of the fact that they give access to higher apparent shear rates under still stable flow conditions (i.e. in terms of pressure drop) than possible at more general flow conditions, they open up prospects towards a widened understanding of flow instabilities as applicable also under more general circumstances. It is to this issue of flow instabilities, as accessed through the present 'window rheology', that we shall turn in the next paper in this series.

CONCLUSIONS

The varied and detailed results from experiments with different extrusion constellations, geometries and construction materials reaffirm the conclusion in our earlier paper[1] that the site of the temperature of reduced flow resistance is the capillary portion of the extrusion geometry, where the effect originates at the wall as a result of a phase transition initiated by simple shear flow induced chain extension. This is in contrast to the previously envisaged elongational flow generated effect within the orifice, which nevertheless still remains the source of flow-induced crystallization at somewhat lower extrusion temperatures. The connection, if any, between the two classes of effect, the rheological temperature window leading to reduced flow resistance and crystallization eventually leading to blockage, originating at two different locations in the system, yet awaits exploration. The new results on the rheological window are all mutually consistent and in quantitative agreement, often down to small details, giving confidence in the above attribution of the effect. The newly explored rheological behaviour within the temperature window, itself as a function of the above variables, widens the existing horizons, both with regard to fundamental studies in rheology and exploitation in practice. The former include access to rates of flow not previously achievable under stable flow conditions in a given material, with newly arising possibilities for exploration and interpretation of the origin of flow instabilities, the subject to be taken up in the next paper in this series.

ACKNOWLEDGEMENTS

Financial support from DSM, The Netherlands, is gratefully acknowledged. We wish to thank Professor T. C. B. McLeish for stimulating discussions.

REFERENCES

1 Kolnaar, J. W. H. and Keller, A. *Polymer* 1994, **35**, 3863
2 Waddon, A. J. and Keller, A. J. *J. Polym. Sci.* 1990, **28**, 1063
3 Narh, K. A. and Keller, A. *Polymer* 1991, **32**, 2512
4 Narh, K. A. and Keller, A. *J. Mater. Sci. Lett.* 1991, **10**, 1301
5 Waddon, A. J. and Keller, A. *J. Polym. Sci., Polym. Phys. Edn* 1992, **30**, 923
6 van der Vegt, A. K. and Smith, P. P. A. *Adv. Polym. Sci. Technol., Soc. Chem. Ind.* 1967, **26**, 313
7 Bagley, E. B. *J. Appl. Phys.* 1957, **28**, 624
8 McLeish, T. C. B. personal communication
9 Wu, S. 'Polymer Interface and Adhesion', Marcel Dekker, New York, 1982
10 Porter, R. S. and Johnson, J. F. *Trans. Soc. Rheol.* 1967, **11**, 259
11 Southern, J. H. and Porter, R. S. *J. Appl. Polym. Sci.* 1970, **14**, 2305
12 Keller, A. and Machin, M. *J. Macromol. Sci. B* 1967, **1**, 41
13 Keller, A. and Odell, J. A. *J. Polym. Sci., Polym. Symp.* 1978, **63**, 155
14 Odell, J. A., Grubb, D. T. and Keller, A. *Polymer* 1978, **19**, 3713
15 Bashir, Z., Odell, J. A. and Keller, A. *J. Mater. Sci.* 1984, **19**, 3713
16 Bashir, Z., Odell, J. A. and Keller, A. *J. Mater. Sci.* 1986, **21**, 3993
17 Bashir, Z. and Keller, A. *Colloid Polym. Sci.* 1989, **267**, 116
18 Kolnaar, J. W. H., Keller, A., Zschunke, C., Seifert, S. and Zachmann, H. G. unpublished results
19 Brochard, F. and de Gennes, P.-G. *Langmuir* 1992, **8**, 3033
20 Migler, K. B., Hervet, H. and Leger, L. *Phys. Rev. Lett.* 1993, **70**, 287
21 de Gennes, P.-G. personal communication
22 Clough, S. B. *J. Macromol. Sci. B* 1970, **4**, 199
23 Pennings, A. J. and Zwijnenburg, A. *J. Polym. Sci., Polym. Phys. Edn* 1979, **17**, 1011
24 White, J. L., Han, M. H., Nakajima, N. and Brzoskowski, R. *J. Rheol.* 1991, **35**, 167
25 Narh, K. A., Barham, P. J. and Keller, A. *Macromolecules* 1982, **15**, 464
26 Hikmet, R. A. M., Narh, K. A., Barham, P. J. and Keller, A. *Prog. Colloid Polym. Sci.* 1985, **71**, 32
27 Narh, K. A., Barham, P. J., Hikmet, R. A. M. and Keller, A. *Colloid Polym. Sci.* 1986, **264**, 507
28 Barham, P. J. and Keller, A. *Macromolecules* 1990, **23**, 303
29 Burton, R. H., Folkes, M. J., Narh, K. A. and Keller, A. *J. Mater. Sci.* 1983, **18**, 315